Research Article

Highly sensitive miniature needle PVDF-TrFE ultrasound sensor for optoacoustic microscopy

Yu-Hang Liu,a,b Alexey Kurnikov,c Weiye Li,a,b Pavel Subochev,c and Daniel Razanskya,b,*

aUniversity of Zurich, Institute of Pharmacology and Toxicology and Institute for Biomedical Engineering, Faculty of Medicine, Zurich, Switzerland
bETH Zurich, Institute for Biomedical Engineering, Department of Information Technology and Electrical Engineering, Zurich, Switzerland
cRussian Academy of Sciences, Institute of Applied Physics, Nizhny Novgorod, Russia

Abstract. A wideband sensitive needle ultrasound sensor based on a polarized PVDF-TrFE copolymer piezoelectric film has been developed, which is capable of providing a noise equivalent pressure of 14 Pa and a uniform frequency response ranging from 1 to 25 MHz. Its high sensitivity (1.6 μV/Pa) and compact size were achieved by capitalizing on the large electromechanical coupling coefficient of PVDF-TrFE and minimizing parasitic capacitance in a two-stage amplifier structure. The detection sensitivity of the newly designed sensor outperformed commercially available hydrophones with an equivalent sensing element area by a factor of 9. The sensor has been successfully integrated into a light scanning optoacoustic microscopy (OAM) system with a limited working space. Submicrometer resolution images were subsequently attained from living mice without employing signal averaging. The miniature sensor design can readily be integrated into various OAM systems and further facilitate multimodal imaging system implementations.

Keywords: photoacoustic; microscopy; hydrophone; *in vivo* imaging; multimodality; miniature.

1 Introduction

Piezoelectric transducers are the most common technology for ultrasound (US) detection, having the merits of a simple structure, high sensitivity, and good electromechanical coupling.[1,2] In recent years, piezoelectric transducers have been widely employed for benchtop optoacoustic microscopy (OAM) systems,[3] endoscopes,[4] and head-mounted imaging platforms.[5] Nevertheless, the sensitivity of piezoelectric-based transducers is fundamentally limited by the active sensing area,[2] impeding efficient miniaturization and limiting applicability. All-optical-based US sensors can overcome the above limitations and attain highly sensitive optoacoustic (OA) signal detection with miniaturized sensors.[1,2,6] However, these approaches require additional interrogating laser sources, while detection stability and sensitivity are commonly affected by environmental factors, such as temperature drifts and vibrations.[2] Hence, a straightforward and efficient US sensing solution for space-limited applications is yet to be found.

Optimal US detection arrangement is also key for development and implementation of multimodal imaging systems, e.g., when combining OAM with two-photon, optical coherence, second-harmonic, or US imaging.[7,8] Since optical-acoustic combiners are known to introduce undesirable wavefront distortions in both optical and acoustic paths, transparent lithium-niobate (LiNbO3)-based US sensors have been proposed as a promising alternative for building hybrid imaging systems that combine light and sound.[9] Nevertheless, the high acoustic impedance mismatch of LiNbO3 restricts detection to a relatively narrow frequency band,[9] while its optical performance is further compromised by non-uniform light transmittance at different wavelengths.[1,9] Miniaturization of US sensors may thus facilitate challenging designs combining optical and acoustic paths.

Here we developed a miniature needle US sensor exhibiting significantly higher sensitivity and wider bandwidth compared to commercially available hydrophones with an equivalent sensing area. For manufacturing the sensor, PVDF-TrFE was chosen as the piezo material because of its large electromechanical coupling coefficient, low acoustic impedance, broadband acoustic response, and durability. A two-stage amplifier was designed to minimize the sensor size while noise equivalent pressure (NEP)

*Address all correspondence to Daniel Razansky, daniel.razansky@uzh.ch

was maintained as low as 14 Pa (across 99 MHz bandwidth for the noise level) mostly due to the minimized parasitic capacitance. The needle US sensor was directly placed under a commercial high numerical aperture (NA = 1.0) objective lens for performing light scanning OAM, and its performance was corroborated by both phantom and *in vivo* experiments in mice.

2 Materials and Methods

A schematic diagram of the miniature sensor is shown in Fig. 1(a). The US sensor was fabricated based on a 20 μm thick film made of a polarized PVDF-TrFE copolymer (PolyK, United States), which was attached to a signal conductor (<1 mm thickness with a diameter of 0.5 mm) via a thin layer of adhesive coating. The conductor edge and signal wire were both covered with insulation, whereas the outer surface of the thin film was deposited with a layer of chromium and aluminum for sensor protection. The main needle US receiver part was shielded in a metal case with an outer diameter of 1 mm and a length of 6 mm, designed with the specific purpose of fitting into a tight space. A two-stage amplification design was employed to ensure a compact needle sensor size by placing the amplifier at one distal end of the transmission cable [Fig. 1(a)]. The needle US receiver was directly linked to a 3 mm × 7 mm × 2 mm size preamplifier, which was placed in a waterproofing case having 4 mm diameter and 10 mm length [Fig. 1(a)]. The preamplifier could provide a high input impedance within a wide (from 1 to 100 MHz) frequency band to match the electrical impedance of the piezoelectric film, which boosted the acquired weak electrical signals to an adequate level before transmission while maintaining minimal noise levels. The preamplifier was connected through an ~20 cm long microcoaxial cable to a low-noise high-frequency operational amplifier to provide a uniform 30-fold amplification within the frequency band from 1 to 100 MHz and introduce negligible parasitic capacitances to the entire electrical circuit. Also the sensor exhibits a relatively low capacitance of 2 pF, sustaining a high electrical voltage generated by the piezo film. A high-pass filter was installed between the preamplifier and amplifier to suppress low-frequency (<1 MHz) components of the input signal, thus reducing pyroelectric signals occurring from reflected photons. The US sensor was supplied with 5 V direct current power.

Performance of the miniature needle US sensor was first demonstrated by evaluating signals generated by illuminating a thin black tape with a focused 532 nm laser pulse [Fig. 1(b)]. The OA signal was detected without averaging exhibiting signal-to-noise ratio (SNR) of more than 25 for per-pulse laser energy of <20 nJ. The sensitivity of the miniature US sensor was then measured in the frequency band from 1.2 to 25.5 MHz and compared with a commercial hydrophone (NH0500, Precision Acoustics, United Kingdom). In order to assess the sensitivity to individual frequencies within the broad detection band, we emitted US waves with three 20 mm disk-shaped piezoelectric transducers (fundamental antiresonant frequencies $f_0 = 1.2, 3.4,$ and 5.1 MHz), made of PZT-19 piezoceramics (Avrora, Russia). For this, the transducers were fed with sinusoidal wave packets of different harmonics using a voltage generator. All measurements were thus carried out for both needle US sensors at f_0 and subsequent odd harmonics (e.g., $3 * f_0$ and $5 * f_0$) of the transducers. The US emitters and both needle US sensors were placed in front of each other spaced by 80 mm in a chamber filled with distilled water [Fig. 2(a)]. The spacing was determined by the boundary of the near Fresnel zone for the fundamental resonant frequency of the US emitting transducers. A trigger signal pulse train with amplitudes (U_{tr}) ranging from 0.1 to 10 V was generated by a function generator (AFG3021, Tektronix, United States) and applied to each US emitter, which filtered the US waveforms to produce the desired harmonic content. The trigger signal consisted of at least 100 cycles to stabilize the emitted US amplitude at resonant
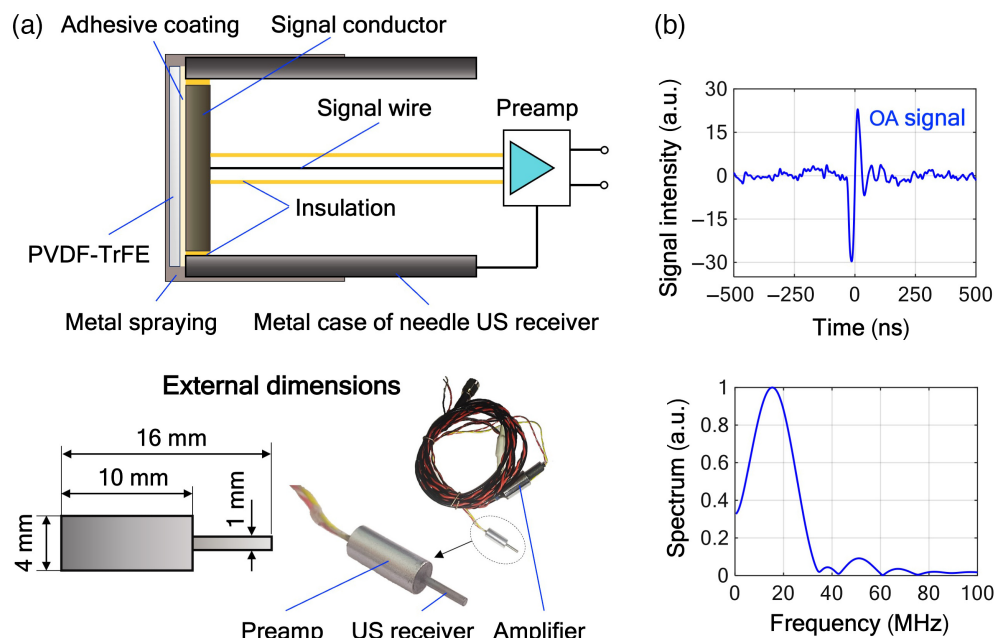

Fig. 1 Design and detection performance characteristics of the miniature needle US sensor. (a) Schematic and external dimensions of the sensor. Preamp, preamplifier. (b) The detected OA signal from a thin black tape and its frequency spectrum.
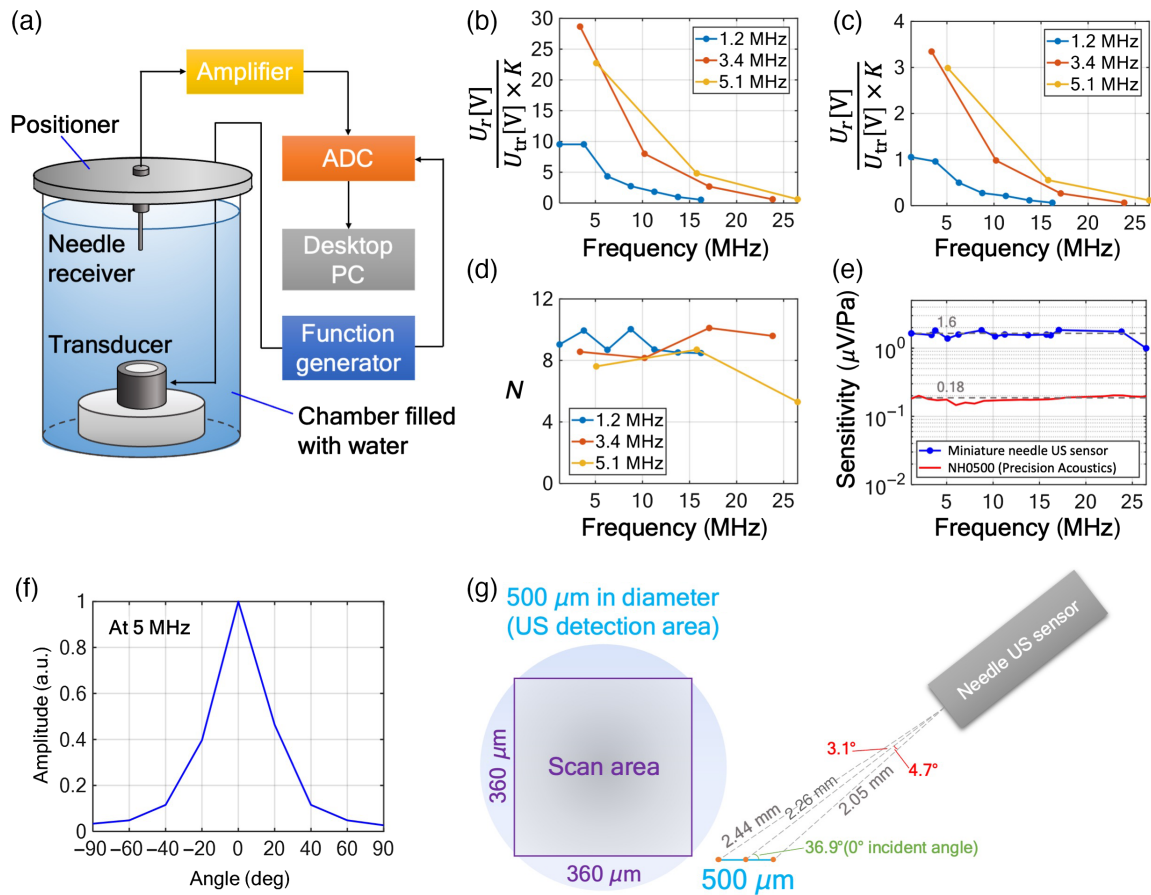
Fig. 2 Sensitivity characterization of the developed needle US sensor and evaluation of the effective US detection area. (a) Schematic of the experimental setup for evaluating the US detection performance. (b) Frequency-dependent normalized signal measurements of the needle US sensor. (c) Corresponding results for a commercial NH0500 hydrophone. (d) Ratio between the curves in (b) and (c). (e) Absolute frequency-dependent sensitivity in μV/Pa. (f) Result of needle US sensor directivity measurements. (g) Schematic of US detection/light scanning area and incident angles for scan points located at the edge of US detection area. The US detection SNR is found to be consistent within this area.

frequencies. The US signals detected by both needle sensors with amplitudes U_r were then recorded and digitized by an analog-to-digital converter (AKIP-75244B, United Kingdom). The measurements were normalized to the excitation voltage applied to the transducers at each resonant frequency and the corresponding preamplifier and amplifier gains when loaded with 50 Ω, namely, $K = 30$ for the proposed PVDF-TrFE sensor in Fig. 2(b) and $K = 2$ for the commercial NH0500 hydrophone in Fig. 2(c). To further compare the sensitivity performance, we calculated the ratio (N) between the frequency responses of the two sensors [Fig. 2(d)]. The result was then multiplied by the known average sensitivity (0.18 μV/Pa) of the commercial NH0500 hydrophone, which was taken from its calibration report. The average sensitivity of the proposed needle US sensor was estimated as 1.6 μV/Pa over the measured frequency bandwidth from 1.2 to 25.5 MHz [Fig. 2(e)], which is about 9 times higher than the corresponding sensitivity of the commercial NH0500 hydrophone. The NEP value for the needle US sensor was subsequently calculated by considering 22 μV root-mean-square (RMS) noise over the amplification bandwidth from 1 to 100 MHz, i.e.,

$$\text{NEP} = \frac{22 \ \mu\text{V}}{1.6 \ \mu\text{V/Pa}} \approx 14 \ \text{Pa}. \tag{1}$$

The enhanced sensitivity of the newly developed needle US sensor can be attributed to a combination of factors, including the two-stage amplification structure, the material properties of PVDF-TrFE, and the diminished parasitic capacitance. The PVDF-TrFE material exhibits a greater electromechanical coupling coefficient (k_t) of about 0.25 as opposed to 0.15 for PVDF, which is an essential factor in obtaining higher sensitivity. In combination with the diminished parasitic capacitance of our needle US sensor (i.e., 1.3 pF versus 9.4 pF for NH0500), this results in the detected electrical voltages being an order of magnitude higher than those measured by the commercial PVDF hydrophone (Table 1). Also the main feature of the developed needle US sensor is the presence of a closely affixed amplifier with a gain of $K = 30$. This helps to pick up and amplify weak signals (e.g., from the smallest capillaries or erythrocytes), further allowing it to withstand electrical interferences, thereby improving the overall SNR. The energy transduction coefficient of the two US sensors was also estimated by

Table 1 Comparison of material properties and measured parameters of two needle US sensors with different piezo thin films.[a]

	PVDF-TrFE (needle US sensor)	PVDF (NH0500)
Thickness (μm)	20	9
Dielectric constant ε	8	13.5
Effective area S (mm^2)	0.2	0.2
Film capacitance C_0 (pF)	0.7	2.6
Measured US sensor capacitance C (pF)	2	12
Electromechanical coupling coefficient k_t	0.25	0.15
Contribution of film capacitance to the total capacitance measurement $\frac{C_0}{C}$	0.35	0.21
Electrical voltage produced by the film $U_0 \cong \frac{1}{C_0}$	1.43	0.38
Electrical voltage produced by the US sensor $U \cong k_t \times U_0 \times \frac{C_0}{C}$	0.1243	0.0127
Energy transduction coefficient $d_{33} \times g_{33} = \frac{1}{\rho v^2} \frac{k_t^2}{1-k_t^2}$ (10^{-12} m^2/N)	7.65	2.64
Measured frequency band (MHz)	1.2–25.5	1–26
Average sensitivity (μV/Pa)	1.6	0.18
RMS noise (μV)	22	30
NEP (Pa)	14	166
NEP (mPa/Hz$^{1/2}$)	2.8	33

[a]Estimated sound speed v and density ρ for both PVDF and PVDF-TrFE are 2200 m/s and 1800 kg/m^3, respectively.

considering their thin-film characteristics. The developed needle US sensor exhibited a higher value, suggesting a more efficient energy conversion and superior performance, as shown in Table 1.[2,10]

We performed hydrophone directivity measurements to evaluate the effects of the incident angle of US waves originating from different scan points. The experimental results indicate that the detected amplitudes can be maintained at >90% levels from the peak values for incident angles in the ±5 deg range [Fig. 2(f)]. The small incident angle differences (i.e., 3.1 deg and 4.7 deg) between the central point and edge points of the scan range help to achieve a uniform US sensing performance within the detection area [Fig. 2(g)]. We selected the 36.9 deg tilted angle (i.e., the central point of the scan, considered as 0 deg incident angle) based on the casing shape of the commercial objective lens. Note that the signal attenuation effects due to travel distance variations is negligible, and the SNR difference within the detection area was mostly due to the scanning of the incident laser beam.[11]

We then integrated the proposed needle US sensor with a submicrometer-resolution OAM system based on a high NA scanning two-photon microscope[12] [Fig. 3(a)]. A nanosecond Q-switched laser operating at 532 nm and 10 kHz pulse repetition frequency (Onda 532, BrightSolutions, Italy) was used as the pumping source to generate OA signals. The laser energy was adjusted by a pair of a half-wave plate and a polarizing beam splitter, and its per-pulse fluctuation was monitored by a biased Si photodetector.[13] The laser beams were scanned by a two-axis galvanometric mirror (6215H, Cambridge Technology, United States), sequentially passed through a combination of a scan lens and tube lenses, and a water immersion microscope objective lens (W-Plan Apochromat 20 × /1.0 DIC, Zeiss, Germany) to focus laser beams onto the target.[11,12] The needle US sensor was mounted on a kinematic V-clamp mount (KM100V/M, Thorlabs, United States) for tuning its position

and angle to acquire the generated OA signals with a maximal amplitude, which were then recorded by a 2-channel, 16-bit digitizer (M4i.4420-x8, Spectrum, Germany) and sent to a desktop computer (PC) for further signal processing and image rendering by a custom MATLAB (R2020b, The MathWorks, United States) script. The multifunction data acquisition cards (NI 6110 and NI 6229, National Instruments, United States) were used as the master controller to trigger the laser firing, galvanometric mirrors, and digitizer. Note that all the optical components were mounted on a custom-made three-axis XYZ stage, which was used to identify the region of interest in the XY dimensions and the imaging focal plane in the Z direction.

A previously reported image processing pipeline[14] was adapted to enhance the OAM image quality [Fig. 3(b)]. We first applied a matched filter to the volumetric OAM data sets for maximizing the SNR of each A-scan signal.[15] Afterward, the data sets were converted into maximum intensity projections images along the depth dimension and processed with nonlocal means filtering for image denoising and smoothing.[16] Contrast limited adaptive histogram equalization (CLAHE) and contrast enhancement were then applied to the processed data sets for adjusting the dynamic range and improving the overall contrast. For instance, a 2D raw OA image of *in vivo* mouse brain vasculature is presented in Fig. 3(c), wherein some vessels (solid blue and dashed green arrows) are not identifiable due to low imaging contrast. In contrast, the processed OA image using the optimized pipeline [Fig. 3(d)] highlights the vessels of interest within the entire field of view (FOV), revealing previously unidentified vessels (blue and green arrows) with enhanced contrast.

In vivo performance was evaluated by imaging microvasculature in the mouse ear and brain after craniotomy surgery (four female athymic nude mice, 10-week-old, Charles River, Germany). Anesthesia was introduced via a mixture of isoflurane (4% for induction and 1.5% for maintenance) and oxygen/air (20%/80%) for all *in vivo* experiments, while the body
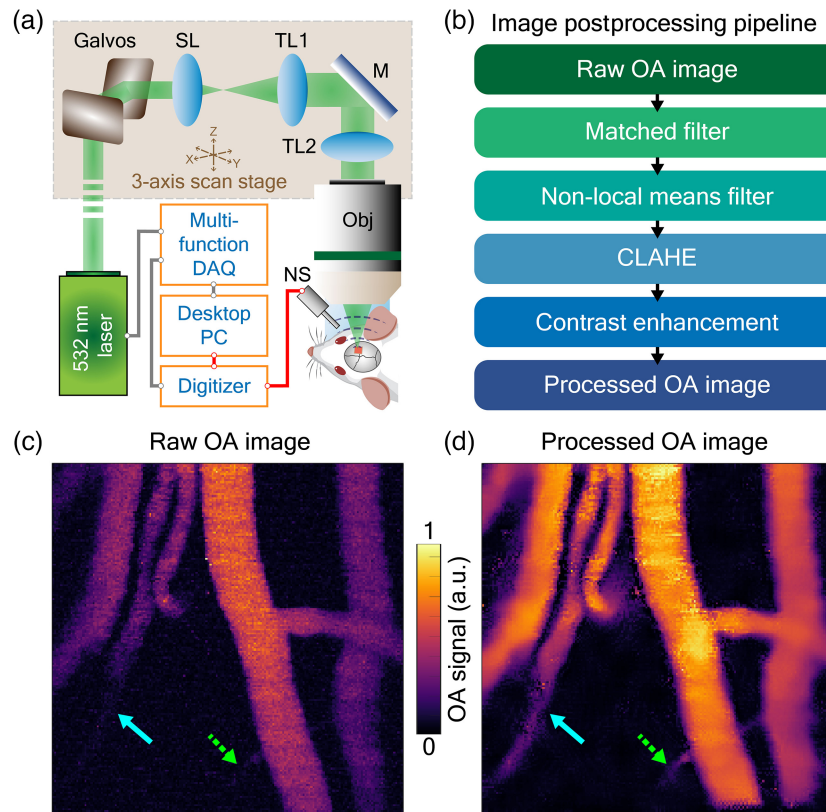
Fig. 3 The customized optical-resolution light scanning OAM system and image postprocessing measures. (a) Schematic of the system. SL, scan lens; TL, tube lens; M, mirror; DAQ, data acquisition card; Obj, objective lens; and NS, needle US sensor. (b) Image postprocessing pipeline; (c) raw OA image; and (d) processed OA image via the optimized image postprocessing pipeline.

temperature and oxygen saturation were constantly monitored by PhysioSuite (Kent Scientific Corporation, United States). During the imaging session, the mouse head was fixed by a head holder (SGM-4, Narishige, Japan), and the imaged region was applied with a small amount of US gel to ensure a good acoustic coupling for OAM imaging. A self-regulated heating pad at 36.8°C was employed to maintain normal mouse body temperature throughout the entire experimental procedure.[13,14] Mice were housed under a 12-h-light/dark cycle, 20°C–24°C temperature, and 50%–70% humidity under specific pathogen-free conditions and received food and water ad libitum. Mouse maintenance and all animal experiments in this study were approved by the local veterinary authority (Kantonales Veterinäramt Zürich, Switzerland).

3 Results

Spatial resolution of the OAM system was characterized by imaging of a surgical blade [Fig. 4(a)] and 7 μm diameter carbon fibers in 1% agarose [Fig. 4(b)]. The experiments were performed with 9–11 nJ per-pulse laser energies, while the images were presented without signal averaging. The lateral resolution was estimated at 0.52 μm by calculating the full width at half maximum (FWHM) of the edge spread function, i.e., derivative of the intensity profile across the blade edge.[11] The effective axial resolution was estimated at 3.73 μm by performing a step scan along the Z direction using a high precision piezo stage.[11,12] It is dominated by the depth of field (DOF) of the optical focus[8]

due to the high NA (NA = 1.0) of the objective lens. The carbon fibers were imaged by a single lateral scan without performing a depth scan, and the reconstructed OAM image [Fig. 4(b)] clearly discerns the individual fibers with high SNR, even at the overlapping intersections. Despite the very short DOF of the scanning OAM, the weaker signals generated by the unfocused illumination at shallower (dashed green arrow) and deeper (solid blue arrow) regions relative to the focal plane were still detectable by our needle US sensor, corroborating its high sensitivity and low NEP.

The broad bandwidth and high sensitivity of the miniature US sensor are supported by the fact that both large vessels and microcapillaries are visible in the images without employing any signal averaging or depth scans [Figs. 4(c) and 4(d)]. In addition, individual red blood cells within a microvessel were also captured by the OAM system, as indicated by the yellow arrowheads in Fig. 4(c). The per-pulse laser energies delivered to the imaged tissues were measured as ~117 and ~51 nJ for the mouse ear and brain vasculature measurements, respectively. The pulse width was ~3 ns as the pulse repetition rate fixed at 10 kHz. The approximate distance between the US sensor and the imaging targets was 2.2–2.3 mm. Note that in the former case,[14] the nanosecond laser was tightly focused on the blood vessels within the highly scattering dermis layer located from 20 to 30 μm underneath the epidermis layer (i.e., the skin surface), which corresponds to ~5.97 mJ/cm^2 light fluence on the ear surface. For brain vasculature, the laser energy was focused on the blood vessels from 15 to 20 μm underneath the brain
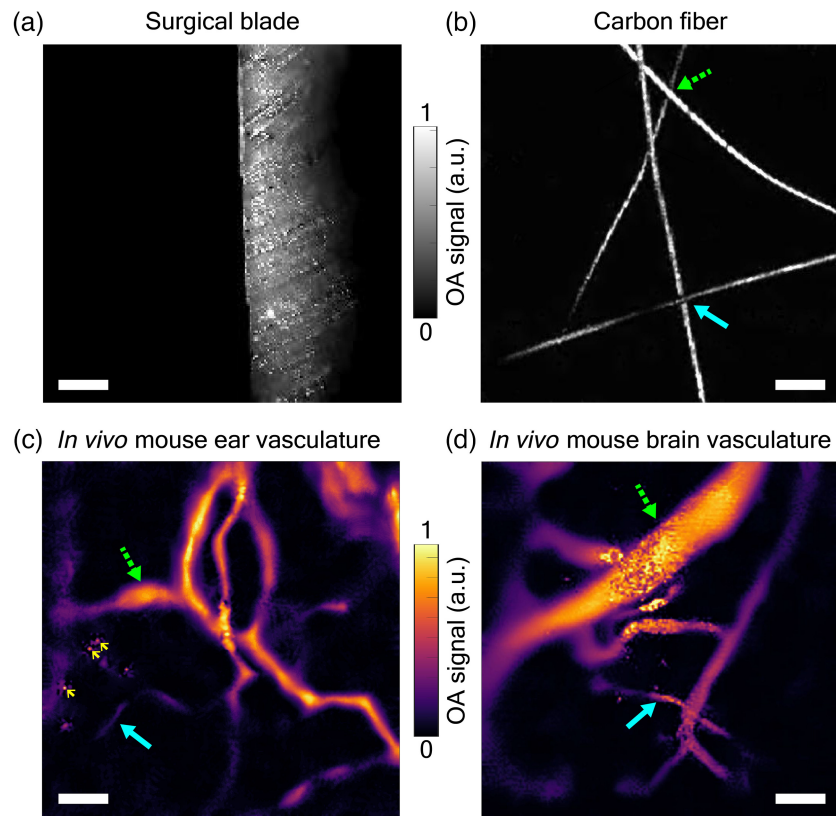
Fig. 4 Images acquired by the light scanning-based OAM system integrated with the needle US sensor. (a) OAM image of a surgical blade; (b) OAM image of 7 μm diameter carbon fibers; (c) *in vivo* image acquired from a mouse ear; and (d) *in vivo* mouse brain vasculature image. The green dashed arrows in (c) and (d) denote large (~29–46 μm diameter) vessels, whereas blue solid arrows denote ~3–7 μm diameter microcapillaries. The yellow arrowheads indicate individual red blood cells within a microvessel. Scale bars: 50 μm.

surface, with the light fluence measuring at ~5.30 mJ/cm². In both cases, the light fluences levels lay within the American National Standards Institute laser safety limits for the 532 nm wavelength.[8] We observed no bleeding or other tissue damage during the *in vivo* experiments.

4 Discussion

In this work, a sensitive and low-cost miniature US sensor was devised based on a PVDF-TrFE film as the US sensing material. By combining the sensor with a two-stage amplifier pair and low parasitic capacitance, high sensitivity and low NEP were achieved. Based on the characteristically broadband acoustic response and low acoustic impedance of the PVDF-TrFE film,[2] we were able to simplify its manufacture procedures by averting the addition of matching and damping layers while preserving good SNR performance. Owing to its miniature design, the proposed needle US sensor could be readily placed at a short distance under a high NA objective lens of the light scanning OAM, avoiding any interference between the sensor and the focusing light path. This facilitates the detection of high-frequency components in the generated OA signals, which are otherwise attenuated heavily after traveling over longer distances.[6] The needle US sensor could be potentially integrated with any wearable OAMs[5] or certain endoscopic imaging devices for specific applications, such as *in vivo* rabbit rectum investigations,[4] thus

also maximizing the flexibility of choosing commercial objective lenses with diverse configurations depending on the needs of a particular biological application. The simple sensor design allows for an easy hybridization with other imaging modalities sharing the same optics, such as two-photon microscopy techniques,[8,12] offering complementary imaging contrasts within the same FOV. It is worth noting that the size of the US sensing part can potentially be further reduced by placing the preamplifier at the rear end and connecting it to the PVDF-TrFE thin film using longer microcoaxial cable, thus offering a more convenient solution for miniaturized devices.

The nonuniform SNR difference across the field predominantly stems from the galvo scan employed in the current light scanning-based OAM system. To address this issue, a calibration procedure can be performed based on a uniform phantom target, providing a thorough understanding of the combined effects of uneven light illumination and OA intensity variations observed at different scan points. Through this approach, adequate compensation for the contrast of reconstructed images can be achieved during the postprocessing stage. Additionally, optimizing the system light path through simulations would ensure a consistent distribution of light across both central and peripheral regions, thereby improving the overall performance of the imaging system. To further expand the FOV of the current setup, an objective lens with a lower NA (e.g., NA = 0.5) can be employed, as the US detection amplitude remains above

80% of the peak values for incident angles within the ± 10 deg range (i.e., equivalent to ~1 mm diameter US sensing area). Furthermore, using the current motorized XYZ scanning platform with a fine step size of 1 μm, one has the capability of physically moving the scanning device, hence covering a larger area. The captured images can then be combined using stitching algorithms to create a comprehensive composite image with an expanded FOV.

In summary, we developed a highly sensitive wideband needle US sensor for high-performance optical resolution OAM imaging. Future research will evaluate alternative piezo materials and optimize the matching and backing layers to further enhance sensitivity. Other promising research directions include the application of the sensor toward design of miniaturized multimodal combinations with other optical microscopy techniques to facilitate functional imaging of brain activity and address a broad range of other biological applications.

References

1. D. Ren et al., "A review of transparent sensors for photoacoustic imaging applications," *Photonics* **8**(8), 324 (2021).
2. G. Wissmeyer et al., "Looking at sound: optoacoustics with all-optical ultrasound detection," *Light Sci. Appl.* **7**, 53 (2018).
3. J. Yao et al., "High-speed label-free functional photoacoustic microscopy of mouse brain in action," *Nat. Methods* **12**(5), 407–410 (2015).
4. H. Guo et al., "Photoacoustic endoscopy: a progress review," *J. Biophotonics* **13**(12), e202000217 (2020).
5. H. Guo et al., "Detachable head-mounted photoacoustic microscope in freely moving mice," *Opt. Lett.* **46**(24), 6055–6058 (2021).
6. S. M. Maswadi et al., "All-optical optoacoustic microscopy based on probe beam deflection technique," *Photoacoustics* **4**(3), 91–101 (2016).
7. M. Seeger et al., "Pushing the boundaries of optoacoustic microscopy by total impulse response characterization," *Nat. Commun.* **11**(1), 2910 (2020).
8. W. Song et al., "Fully integrated reflection-mode photoacoustic, two-photon, and second harmonic generation microscopy in vivo," *Sci. Rep.* **6**, 32240 (2016).
9. J. Park et al., "Quadruple ultrasound, photoacoustic, optical coherence, and fluorescence fusion imaging with a transparent ultrasound transducer," *Proc. Natl. Acad. Sci. U. S. A.* **118**(11), e1920879118 (2021).
10. Y. Liang et al., "Optical-resolution functional gastrointestinal photoacoustic endoscopy based on optical heterodyne detection of ultrasound," *Nat. Commun.* **13**(1), 7604 (2022).
11. Y. H. Liu et al., "Sensitive ultrawideband transparent PVDF-ITO ultrasound detector for optoacoustic microscopy," *Opt. Lett.* **47**(16), 4163–4166 (2022).
12. J. M. Mayrhofer et al., "Design and performance of an ultra-flexible two-photon microscope for in vivo research," *Biomed. Opt. Express* **6**(11), 4228–4237 (2015).
13. Y. H. Liu et al., "Non-invasive longitudinal imaging of VEGF-induced microvascular alterations in skin wounds," *Theranostics* **12**(2), 558–573 (2022).
14. J. Rebling et al., "Long-term imaging of wound angiogenesis with large scale optoacoustic microscopy," *Adv. Sci.-Weinh* **8**(13), 2004226 (2021).
15. S. W. Smith, "Chapter 17: custom filters," in *Digital Signal Processing*, S. W. Smith, ed., pp. 297–310, Newnes, Boston (2003).
16. A. Buades, B. Coll, and J. M. Morel, "A non-local algorithm for image denoising," in *Proc. CVPR*, IEEE, pp. 60–65 (2005).

Yu-Hang Liu received his PhD in electrical and computer engineering from the National University of Singapore in 2017. He is currently working as a postdoctoral fellow in Prof. Daniel Razansky's group at the University of Zurich and ETH Zurich, Switzerland. His primary research focuses on the advancement of innovative multimodal optoacoustic imaging systems for various *in vivo* biomedical applications. He has published 24 peer-reviewed journal articles and 1 book chapter.

Alexey Kurnikov is a junior researcher in the laboratory of ultrasonic and optoacoustic diagnostics at IAP RAS. He received MS in radiophysics in 2021 from Lobachevsky State University of Nizhni Novgorod.

Weiye Li obtained the MSc degree in electrical engineering and information technology from ETH Zurich, Switzerland, in 2019. He is currently a PhD candidate under the supervision of Prof. Daniel Razansky at the University and ETH Zurich. His research focuses on image reconstruction and processing methods for quantitative optoacoustic imaging.

Pavel Subochev is the head of the laboratory of ultrasonic and optoacoustic diagnostics at IAP RAS. Since 2012, he has been focused on the development of new instrumentation for optoacoustic imaging of biological tissues.

Daniel Razansky is a full professor of biomedical imaging with double appointments at the Faculty of Medicine, University of Zurich, and the Department of Information Technology and Electrical Engineering, ETH Zurich. His lab has pioneered and commercialized several imaging technologies, among them the multispectral optoacoustic tomography and hybrid optoacoustic ultrasound imaging. He has authored over 300 peer-review journal articles and holds 15 patented inventions in bio-imaging and sensing. He is fellow of IEEE, SPIE, and Optica.